A CFD ANALYSIS OF THE IMPINGEMENT COOLING EFFECT OF THE COOLANT JET CAUSED BY THE T56 1ST STAGE DISC METERING HOLE

ISABE-2003-1065

Glen C. Snedden
CSIR, Defencetek, P O Box 395
Pretoria, 0001, South Africa
Tony Lambert
Rolls-Royce
Indianapolis, Indiana, USA

Abstract

This investigation examines the results of the CFD analysis of the effect of coolant impingement on the back of a disc (or wheel) as part of the secondary cooling circuit of the T56-A-15LFE turboprop engine.

As part of the collaborative study involving Rolls-Royce, CSIR and NRC of Canada performed a conjugate heat transfer analysis using techniques developed through experience with other South African Air Force (SAAF) engines [1], boundary conditions and geometrical detail supplied by Rolls-Royce [2] and the commercial CFD code Star-CD®.

The results of the analysis indicate that the effect, although clearly visible on used parts (Figure 1), is localized and confined to the metal surface. This, coupled with the isolation of the impingement zone (far from the critical stress locations) meant that the impingement effect was not considered in the calculation of aerothermal boundary conditions for the life assessment study of these components.

Introduction

The construction of the T56-A-15LFE turbine section consists of 4 discs and 3 spacers. Spacers 1-2 and 3-4 are shrunk onto the curvic-coupling web of the 1st and 4th discs respectively and located using steel pins. The entire assembly is then held together using long tie-bolts. Coolant enters the cavities via metering holes drilled through the curvic-coupling web. As a result of physical restrictions during the manufacturing process these holes are angled toward the face of the disc and result in flow impinging on the rear surface of the 1st disc. Figure 2 shows a section through the relevant components of the first inter disc and spacer cavity, showing the metering hole angular inclination.

Users and engineers at the South African Air Force (SAAF) and CSIR had noted this effect as a result of the noticeable discoloration of the disc, shown in Figure 1. However, the impingement was not featured in the previous empirically based solution of the aerothermal conditions in the secondary flow circuit by Rolls-Royce.

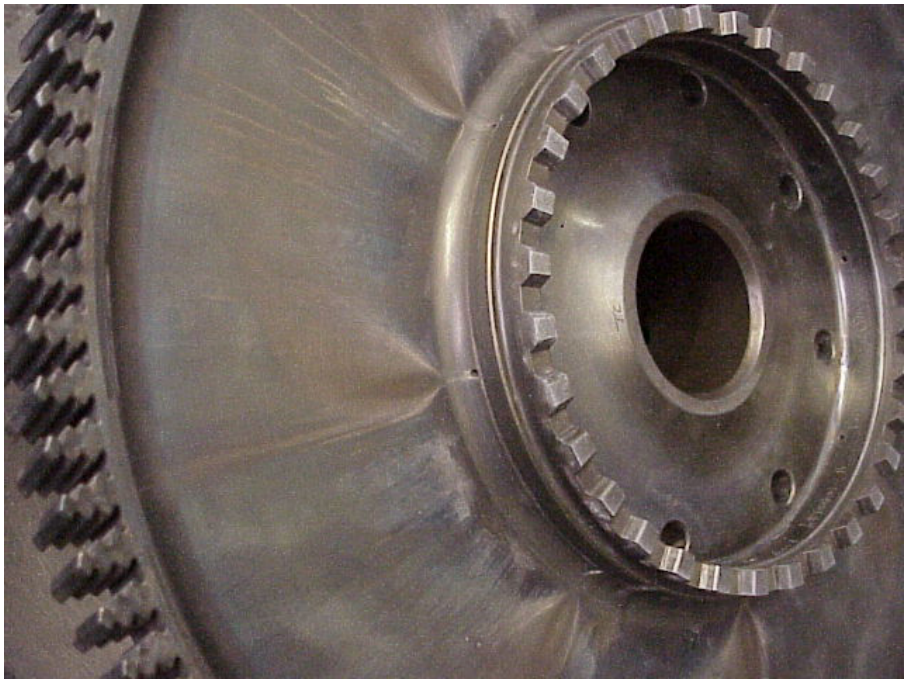

Figure 1: Discolouration of a used 1st stage disc with the metering holes visible

These results are supplied as boundary conditions to the downstream stress analysis in the life assessment process, which was being redone as a result of user concern over the reduction in life of the disc assembly components.

In order to determine the effect of the coolant impingement on the back of the 1st stage disc a CFD analysis was commissioned and performed using the commercial CFD package Star-CD ®. The conjugate heat transfer analysis focused on only one disc cavity and formed a precursor and validity check on the empirical analysis.

Model Geometry

The model geometry was supplied to the CSIR by Rolls-Royce along with the secondary flow circuit conditions [2], necessary for providing boundary conditions, and the material properties for the disc and spacer components. A schematic representation of the geometry and the final boundary conditions used is contained in Figure 2.

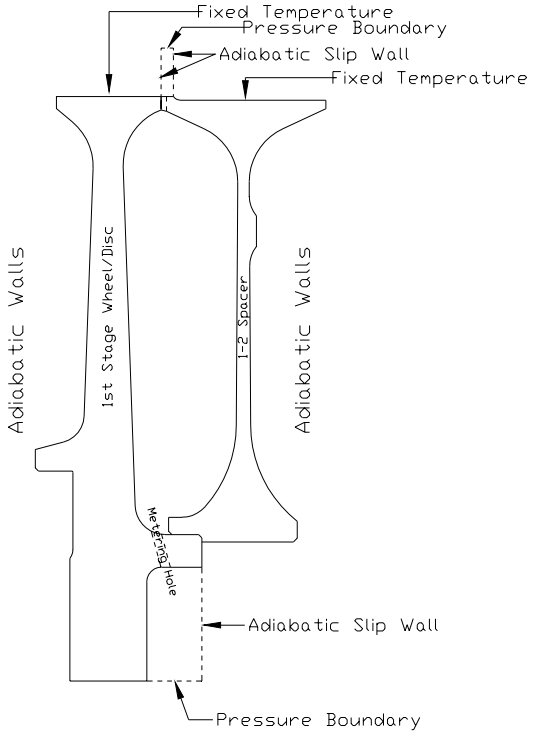

Figure 2: Schematic section of the geometry and boundary conditions applied to the T56 disc and spacer

Modelling Approach

The modelling approach is essentially the same as that discussed in [1], however, in this case the interest area is solely the region where the flow impinges on the disc, hence the geometry modelled was limited to only the one cavity in question and the disc, spacer and enough fluid cells to situate the boundary conditions far enough from the domain to achieve an accurate and stable solution.

Geometrical Assumptions

A 90° sector of the cavity was modelled in order to simultaneously and accurately capture the number of exit ports and inlet jets. A summary of the boundary conditions applied is given in Figure 2.

Figures 3 to 7 give an overview of the final mesh and some idea of the block structured approach and refinement in the main area of interest, that is, the impingement zone and metering holes at the lower part of the cavity. Red cells denote the disc or wheel, green the spacer and blue the fluid cells.

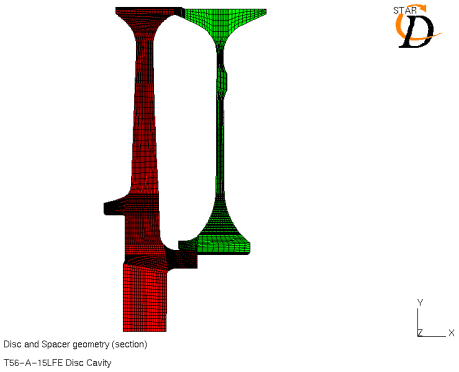

Figure 3: Cross section of the solid components indicating the mesh structure

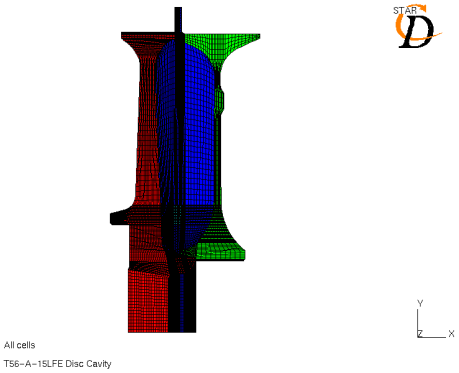

Figure 4: Cross section of the overall domain indicating the mesh structure and corresponding to Figure 2

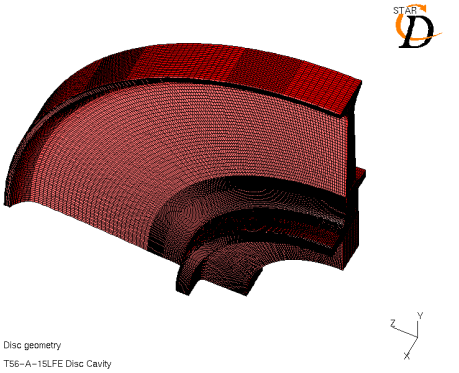

Figure 5: Mesh of the quarter segment of the disc/wheel

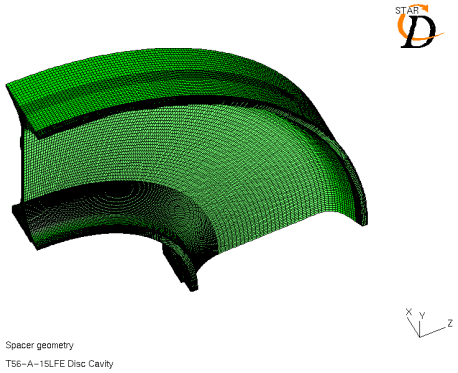

Figure 6: Mesh of the quarter segment of the spacer

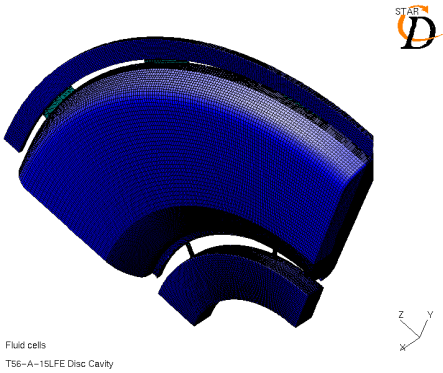

Figure 7: Fluid mesh with the two metering holes (bottom) and three exit scallops (top)

Figures 8 and 9 show the metering hole and exit scallop in closer detail. One-to-one matching of fluid and solid cells was utilized to avoid any matching errors on the inside surfaces of the cavity and wherever else possible. This leads to some unnecessary concentrations of cells, particularly in the solids as a result of the block structured approach. Arbitrary interfaces are only employed in three locations: to match the fluid cells above the disc rim to the exit scallops, to match the fluid cells below the metering holes to metering holes, and between the metering holes and the cavity region. In all cases this removes the arbitrary interface as far as possible from the area of interest or of high impact on the physics of the flow.

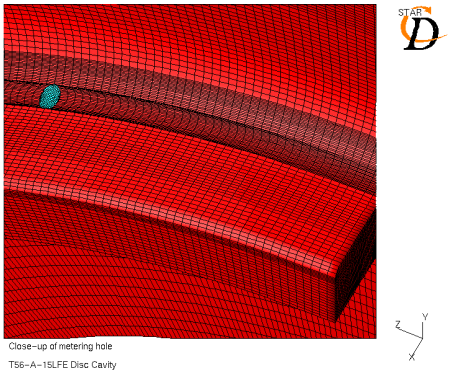

Figure 8: Close-up view of the meshing of one of the metering holes

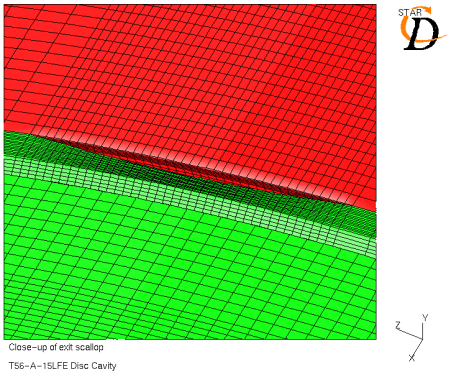

Figure 9: Close-up view of one of the exit scallops

Boundary Conditions and Assumptions

These were supplied by Rolls-Royce [2] and applied as shown in Figure 2. To act as metering holes the entry of the coolant air into the cavity should be choked, this statement provided the first order check for the solution, that is that the flow exiting the metering hole should be sonic. The settings used in the solution are contained in Tables 1 and 2. The default boundaries are adiabatic walls which result in an over prediction of temperature on the upstream side of the disc and downstream side of the spacer as these sides are also cooled. No contact resistance was modelled.

Convergence

Convergence is determined by monitoring the reported temperature of appropriately placed monitoring cells in disc and spacer material. Once no change was indicated after 1000 iterations, the run was stopped.

Table 1: Boundary conditions

Position	Type	Setting
Radial Ends	Cyclic	-
Inlet	Static pressure	0 Pa (relative) 659 K 4 % turbulence intensity
Outlet	Static pressure	468154 Pa (relative)
Vertical surfaces of inlet and outlet blocks	Slip walls	-
Disc rim	Fixed temperature	839 K
Spacer rim	Fixed temperature	883 K

Table 2: Solver settings

Category	Parameter	Settings
Rotating reference frames	Single frame	All materials 13,820 rpm
Thermophysical models	Conjugate heat transfer reference pressure	On 943 892 pa
Molecular properties	Density viscosity specific heat conductivity	Ideal Sutherlands law constant
Turbulence model	High Reynolds, k-ε	Default
Materials properties	Disc Spacer	Waspaloy IN901
Analysis controls	Solution method Solution algorithm	Steady state MARS
Relaxation parameters	All	Default

Flow Solution

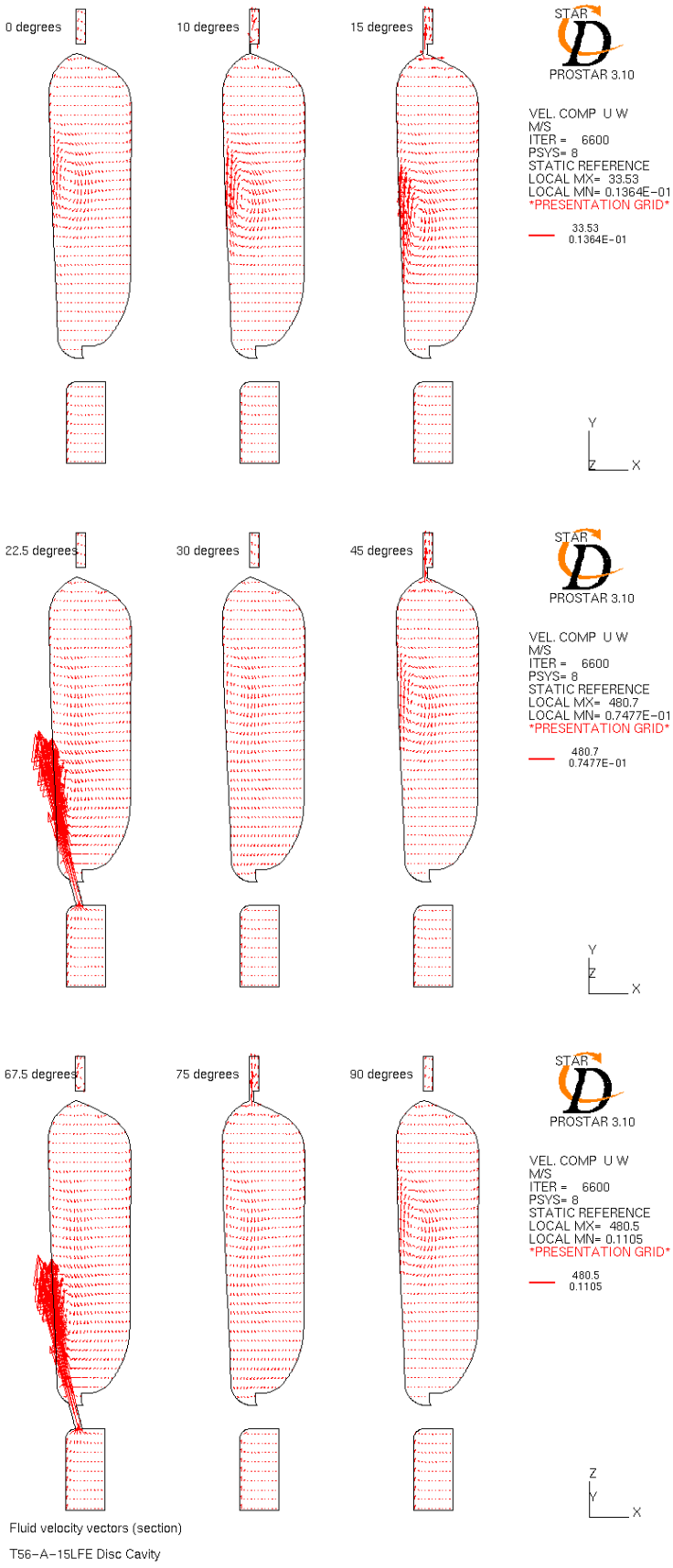

Figure 10: Fluid velocity vectors at various radial sections

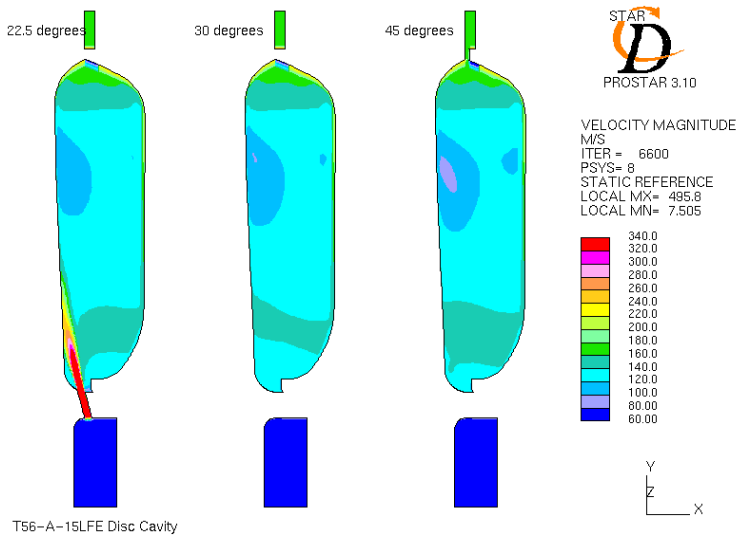

Figure 11: Velocity magnitude contours at selected radial sections

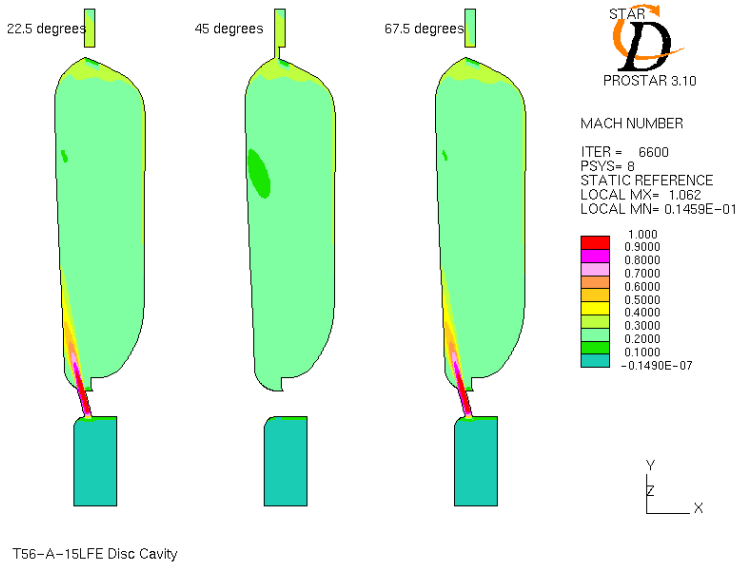

Figure 12: Mach number contours at selected radial sections

Figure 10 shows the flow patterns within the disc cavity. The main feature can be seen to be the high speed jets emanating from the metering holes and impinging on the downstream surface of the disc. This then results in a vortex which rolls up the disc as it dissipates, see sections 22.5, 15, 10 and 0 degrees in that order. The only other features worth mentioning are the viscous drag that is apparent on the walls of both disc and spacer, which results in the boundary layer moving radially upwards, and the flow ejecting via the scallops in the sections at 15, 45 and 75 degrees.

Figures 11 and 12 show velocity magnitude and Mach number contours at a selection of sections, primarily through exit scallops and metering holes. The Mach number plots indicate sonic Mach numbers through the metering holes, which is the desired condition. The discontinuity in the contours on the downstream side of the exit scallops in both Figures 11 and 12 is a result of a large step change in mesh density and subsequent interpolation issues. This is acceptable as the area does not affect the overall mass flow rate and is situated far from the area of interest, which is the impingement zone.

Temperature Solution

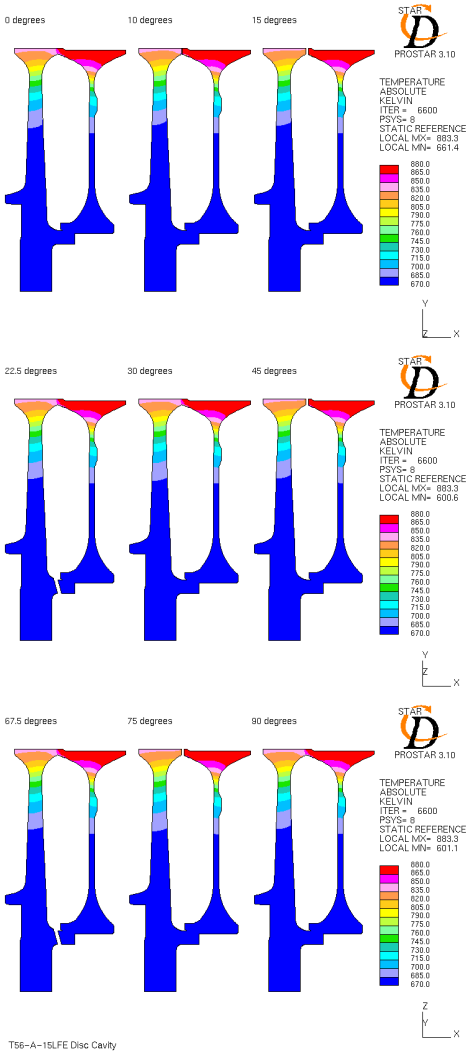

Figure 13: Metal temperature contours, temperature scale 650 K - 880 K, at various radial sections

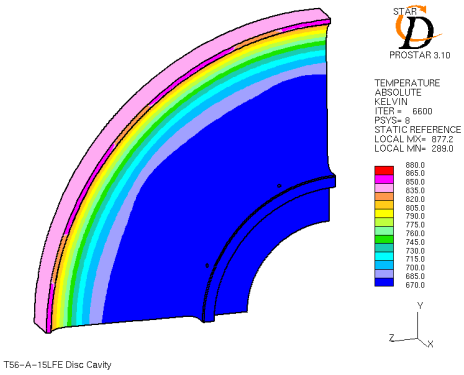

Figure 14: Downstream disc metal temperature: scale 650 K - 880 K

Viewed on a temperature scale that encompasses the entire range of temperatures in the metal, the effect of the impingement of flow from the metering holes is not even noticeable. The dominant effect is the radial conduction of heat down into the disc and spacer, which dissipates rapidly and is essentially removed at half the radius of the spacer, see Figures 13 and 14. The effect of the impingement then lies at a level one colour band below the range on these figures, see Figures 15, 16 and 17.

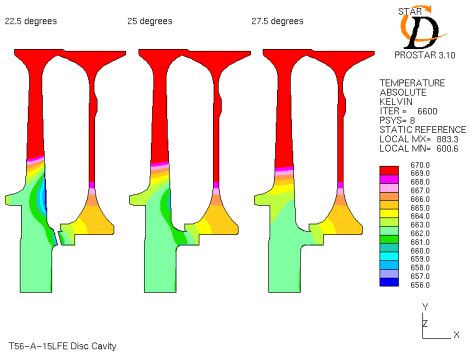

Figure 15: Selected section plots of metal temperature opposite and downwind of the metering hole, temperature scale 656 K - 670 K

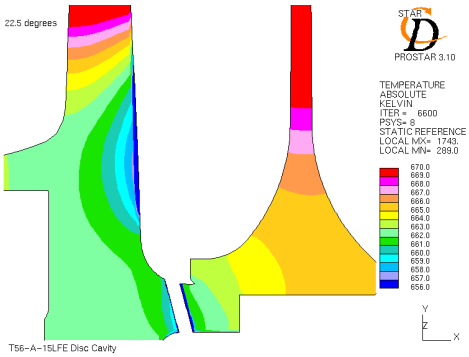

Figure 16: Close-up view of the metal temperature contours opposite the metering hole, scale 656 K - 670 K

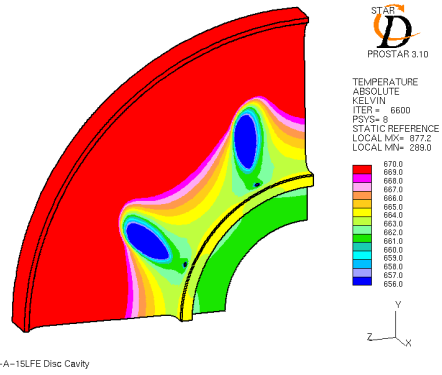

Figure 17: Downstream disc metal temperature, scale 656 K - 670 K

As can be seen in Figures 15 and 17 and in an expanded view in Figure 16, the effect of the coolant jets emanating from the metering holes on the overall temperature of the discs is small, limited to only a few degrees and penetrates to just over half the thickness of the disc in total extent. Add to this the effect of the adiabatic boundary imposed on the upstream surface of the disc which results in an over prediction of the disc temperature and the extent and penetration of the impingement effect is most likely even less.

Figure 18 shows the fluid temperature and the extent of the penetration of the coolant both through the high speed impinging jet and the viscous drag up the face of the disc.

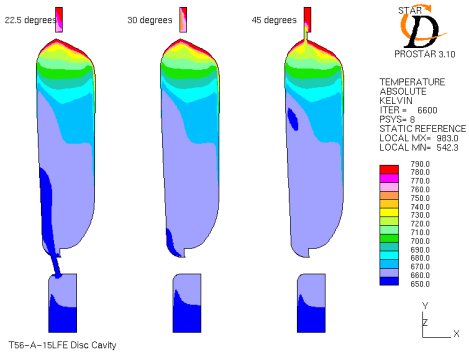

Figure 18: Fluid temperature at selected radial sections

What is evident thus far in the investigation is that the effect of the impingement flow on the disc is clear but small. However, the question remains, does this impact on the life of the components in question? For the disc the answer is that it does not. Not only is the effect small, but it is far from the critical locations. In the case of the spacer there is little effect from the coolant flow, no major circulation of coolant from the disc impacts on the spacer. Figures 19 and 20 indicate the temperature patterns on the spacer on similar scales as those used for the disc. Once again the global pattern shows no effect while Figure 20 shows a slight effect from conduction around the metering holes which is conducted into the spacer through a path which would in reality include some form of slight contact resistance and again mitigates what is a very slight effect.

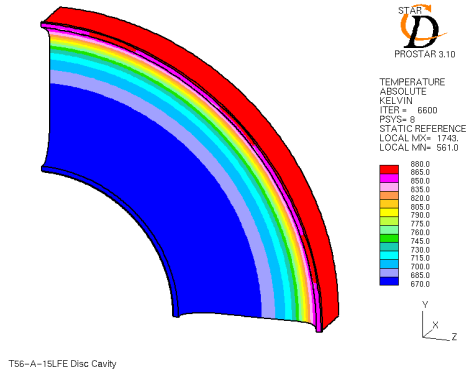

Figure 19: Spacer metal temperature, scale 670 K - 880 K

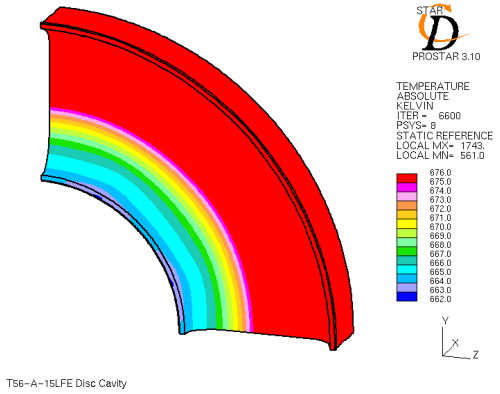

Figure 20: Spacer metal temperature, scale 662 K - 676 K

Therefore, although this effect on the spacer might interfere with one possible critical location in terms of the component life - namely the anti-rotation pin-hole, the effect is extremely small, being in the order of less than 2 K.

Heat Transfer Coefficients

The heat transfer coefficients shown in Figure 21 give clear correlation to the footprints noted by the CSIR and South African Air Force (SAAF), however the effect is thought not to be thermal due to the lack of meaningful temperature difference. Instead the effect is felt to be the result of surface polishing by dust particles combined with surface corrosion effects, which would require a microstructure analysis to confirm.

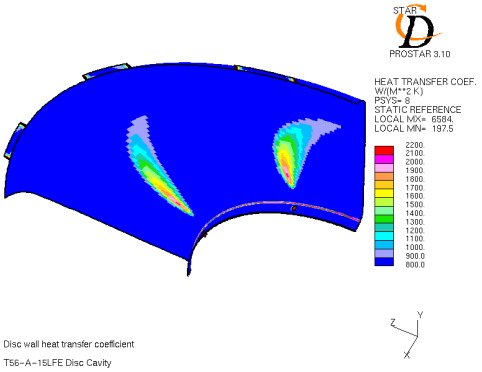

Figure 21: Heat transfer coefficient on the downstream surface of the disc

Figure 22 indicates the y+ or near wall Reynolds number values on the disc, which are higher than recommended (30 to 100 for the turbulence model used) but significantly better than earlier attempts at such work, for example [1]. The majority of the disc face and particularly in the impingement area lie in the range 10 to 140 y+.

Conclusions

The results of the study conclusively showed the effect of the impingement jet to be of little significance when compared to the dominant radial conduction temperature profile of the disc. The heat transfer pattern qualitatively matches the pattern visible on the disc, in part validating the results. However, the temperature differential between the coolant flow and impingement area results in a thermal footprint of only a few degrees and with little overall effect.

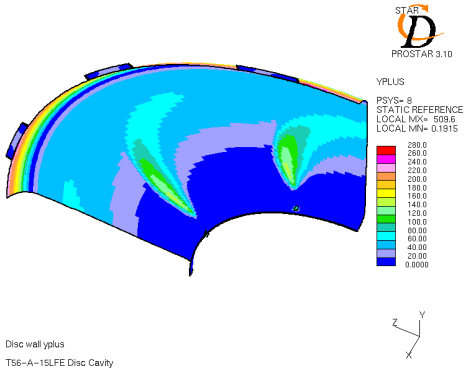

Figure 22: Y+ values on the downstream surface of the disc

Armed with this information the effect of the impingement jet was not considered in the 2D empirical analysis that followed at Rolls-Royce, as the thermal stresses resulting from the small temperature differences found were believed to be negligible and in an area devoid of other stress raisers and hence not a critical location for the life of the component.

Acknowledgements

Jeffery Baloyi who helped set up and run the final case during his vacation work and Brian Cannoo and Thomas Roos for their insight into the mechanics of the code and fluid solution respectively.

References

[1] G Snedden (2003) *Simplified 3D Simulation of a Turbojet Disc Cavity with Conjugate Heat Transfer* ISOABE 2003-1179

[2] Rolls-Royce (2000) *T56-A-15LFE Secondary Flow Primer*

[3] Computational Dynamics (1999) *User Guide* Version 3.10